

Active Gel Theory for Cell Migration With Two Myosin Isoforms

Nils O. Winkler,¹ Oliver M. Drozdowski,^{1,2} Falko Ziebert,¹ and Ulrich S. Schwarz^{1,2,*}

¹*Institute for Theoretical Physics and Bioquant, Heidelberg University, 69120 Heidelberg, Germany*

²*Max Planck School Matter to Life, Heidelberg University, 69120 Heidelberg, Germany*

(Dated: February 18, 2025)

Myosin II molecular motors slide actin filaments relatively to each other and are essential for force generation, motility and mechanosensing in animal cells. For non-muscle cells, evolution has resulted in three different isoforms, which have different properties concerning the motor cycle and also occur in different abundances in the cells, but their respective biological and physical roles are not fully understood. Here we use active gel theory to demonstrate the complementary roles of isoforms A and B for cell migration. We first show that our model can be derived both from coarse-graining kinetic equations and from nonequilibrium thermodynamics as the macroscopic limit of a two-component Tonks gas. We then parametrize the model and show that motile solutions exist, in which the more abundant and more dynamic isoform A is localized to the front and the stronger isoform B to the rear, in agreement with experiments. We then explore the parameter space of the model and find a general pull-and-push mechanism that can produce different migratory modes, including cell oscillations in length and velocity. We also describe an analytical solution for the stiff limit. Our findings highlight the importance of including isoform-specific molecular details to describe whole cell behavior.

I. INTRODUCTION

Cell migration is an essential process for any living organism. In multicellular animals like humans, it is important mainly for embryonic development [1], wound healing [2] and the immune response [3], but also for the spread of cancer [4]. It is strongly linked to the underlying molecular processes, because cells have to generate force and movement that is converted into consistent migration on the cell scale. This function is provided by the cytoskeleton, a collection of polymer networks. Cells can push their envelope forward by polymerization of these filaments. They also can generate pulling forces by sliding them relative to each other with molecular motors. For animal cells, pushing and pulling forces are generated mainly by actin filaments and myosin II molecular motors. In cell migration, they go hand-in-hand, because the actin networks generated by polymerization are pulled backwards by myosin II motors. The resulting retrograde flow is then transmitted to the substrate by adhesions and thus generates forward motion of the cell [5]. Migration requires a cyclic process that converts energy provided in the form of ATP into force and movement. Moreover, initiation of motility requires a symmetry break between front and back, which can be either spontaneous or driven by some external cue [6–8]. Usually this break of symmetry is related to activation of the Rac/Cdc42 and RhoA pathways, which for quantitative experiments can be controlled by optogenetics [9–11].

In non-muscle animal cells contractile stress for cell motility is produced by motor proteins of the non-muscle myosin II (NMII) family [13]. Evolution has resulted in three isoforms, namely NMIIA, NMIIB and NMIIC [14].

After activation of the Rho-pathway, the myosin motors are assembled into mini-filaments that typically mix different isoforms [14, 15]. These mini-filaments then bind to the actin cytoskeleton, generate stress and at the same

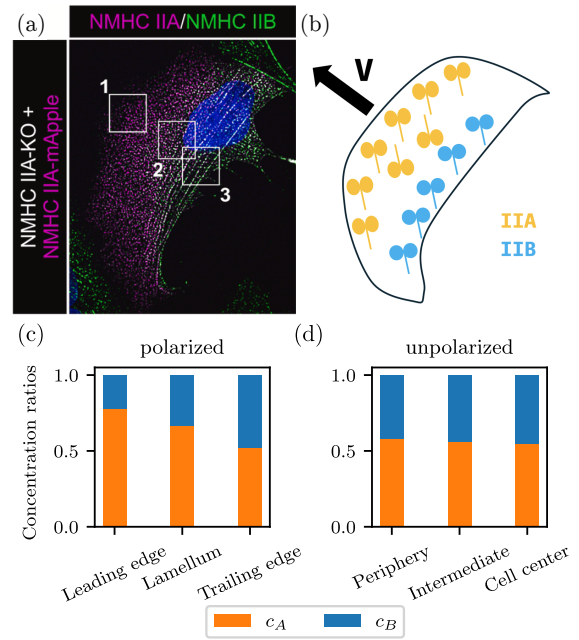


FIG. 1. NMII isoform distributions in cells. (a) Microscopy image of a U2OS cell with exogenous NMIIA (magenta) and endogenous NMIIB (green). Modified from [12]. (b) Schematic sketch of a cell indicating NMII isoform distribution and net cell movement. (c), (d) Experimental concentration ratios of NMIIA and NMIIB within different cell compartments (c: along the axis of polarization, d: unpolarized cell). Adapted from [12]. While both isoforms are equally distributed in an unpolarized cell, in a moving cell NMIIA and NMIIB enrich at the leading and trailing edges, respectively.

* Corresponding author: schwarz@thphys.uni-heidelberg.de

time are advected with the resulting cytoskeletal flow. In the case of asymmetric contractile stress distributions, the cell is polarized and starts migrating. While NMIIA is most abundant and propels loads the quickest along actin filaments, NMIIB is the strongest due to its higher duty ratio; NMIIC seems to have little relevance for cell migration, also due to its low abundance [12, 16]. Recent experiments have shown that in a migrating cell the isoforms A and B are not distributed equally [12, 15]. While the more abundant and more dynamic isoform A localizes more at the leading edge, the stronger isoform B accumulates towards the trailing edge (cf. Fig. 1).

In the following, we will define and analyze a model that considers the complementary roles played by the two dominant isoforms A and B. We use active gel theory, which models the contractile actomyosin network as an active viscous material and thus is a natural approach to describe flowing actin networks as the physical basis of cell crawling [17, 18]. In principle, active gel theory can describe the effects of both actin polymerization and myosin-based contractility, but seminal work has shown that contractility alone is sufficient to explain cell migration [19–21]. While this minimal model leads to a supercritical pitchfork bifurcation towards a motile state, more recently it was shown that a subcritical pitchfork bifurcation and bistability can be obtained when including a non-linearity in the diffusion behavior, which can be derived from the physics of a van der Waals fluid [22].

Here we extend this approach to a theory for two species of NMII. Motivated by experiments by Weisenbruch et al. [12, 16], we incorporate phenomenological binding kinetics, including the competition of isoforms A and B for binding sites on actin filaments. This amounts to a volume exclusion interaction and results in an effective non-linear diffusion of myosins as known from the Tonks gas [23]. Our new model explains the experimentally observed distributions of NMIIA and NMIIB in a polarized migrating cell. Exploring the parameter space we can describe four different modes of cell motility: non-motile cells, decaying and stable pull-push velocity oscillations, and motile steady migration. Using both numerical simulations and analytical theory, we can obtain a complete phase diagram for our model.

The paper is organized as follows. We will start by defining the mathematical model based on active gel theory introducing the constitutive relation for stress. From binding kinetics we derive an effective nonlinear diffusion and demonstrate its consistency with the thermodynamics of a Tonks gas of two species. We then investigate the resulting closed boundary value problem and recapture experimental results in steady-state. Lifting the constraint of steady-state we demonstrate an oscillation mechanism for cell length and velocity. Lastly, we introduce a limiting case which can be treated analytically and for which we present a phase diagram indicating four different modes of motility.

II. MINIMAL CELL MODEL WITH TWO MYOSIN ISOFORMS

A. Geometry and Mechanics of the cell

Our one-dimensional model considers an infinitely compressible active gel. As commonly assumed [20, 22], the active contractile stress depends linearly on the motor concentration c , $\sigma_{act} = -\chi c$, resulting in the constitutive relation

$$\eta \partial_x v(x, t) = \sigma(x, t) - \chi_A c_A(x, t) - \chi_B c_B(x, t). \quad (1)$$

Here $v(x, t)$ is the velocity of the actin flow and η the viscosity. The right hand side contains the total stress $\sigma(x, t)$ and the active stresses caused by the myosin concentrations $c_A(x, t)$, $c_B(x, t)$ of the two isoforms. The minus signs relate to contraction and the prefactors χ_A , χ_B quantify the contractility of the species. Since the cell is adhering to the substrate, we assume homogeneous viscous drag and get the force balance

$$\partial_x \sigma = \xi v, \quad (2)$$

where ξ is a friction coefficient. The cell occupies the range $x \in [l_-, l_+]$ and hence its length is given by $L(t) = l_+(t) - l_-(t)$ and its midpoint velocity by $\dot{G}(t) = (v(l_+, t) + v(l_-, t))/2$. We use an elastic boundary condition, $\sigma(l_{\pm}, t) = -k(L(t) - L_0)/L_0$, that models membrane tension and all other restoring forces limiting the cell size [20–22]. Here k is the effective spring constant of the cell and L_0 its homeostatic length.

B. Myosin Motor Binding Kinetics

Myosin motors generate contractile forces by binding to actin. Informed by the myosin cross-bridge cycle [24–27], we can formulate equations for their dynamic behavior. Although the cross-bridge cycle consists of multiple steps, we will solely distinguish between motors that are either attached to (index a) or detached from (index d) actin filaments to create an effective two-state model as considered in [20, 22, 28].

In the unbound state, the motors can freely move inside the cytoplasm with diffusion constant \bar{D} and bind to actin at a rate k_{on} . The binding process is subject to volume exclusion effects, i.e. there must be a free spot available on the actin filament to be able to bind. This is modeled by introducing a saturation concentration c_{∞} . When it is reached locally, no more binding is possible. The attached proteins move with the (retrograde) actin flow by advection with the velocity v . Since the cytoplasm is considered as a reservoir for the motors, the detachment rate k_{off} is assumed to be independent of any interaction effects. In general, the binding rates are specific for each isoform ($k_{A,on/off} \neq k_{B,on/off}$). In contrast, both the diffusion coefficient and the saturation concentration are mostly determined by the size of the protein

which is the same for both isoforms. This leads to the following two differential equations per isoform

$$\partial_t c_{i,a} + \partial_x(v c_{i,a}) = R(c_{i,a}, c_{i,d}), \quad (3a)$$

$$\partial_t c_{i,d} - \tilde{D} \partial_x^2 c_{i,d} = -R(c_{i,a}, c_{i,d}), \quad (3b)$$

$$R(c_{i,a}, c_{i,d}) = \frac{k_{i,\text{on}}}{c_\infty} (c_\infty - (c_{i,a} + c_{j,a})) c_{i,d} - k_{i,\text{off}} c_{i,a}. \quad (3c)$$

Here $R(c_{i,a}, c_{i,d})$ is a nonlinear function describing the reaction kinetics and i, j refer to isoforms A and B, respectively. For the cellular behavior on the time scale of interest here, we do not include a production of myosin inside the cell, but rather require the total myosin concentration of each isoform to remain constant. This requirement then leads to no-flux boundary conditions for the two species, $\partial_x c_{A,B}(l_\pm, t) = 0$.

We now simplify the problem, as previously proposed for similar models [20, 22]. First, we assume local chemical equilibrium, $R(c_a, c_d) = 0$, and obtain expressions for the detached motors

$$c_{i,d} = \frac{1}{K_i} \cdot \frac{c_{i,a} c_\infty}{c_\infty - (c_{i,a} + c_{j,a})}, \quad (4)$$

where $K_i = k_{i,\text{on}}/k_{i,\text{off}}$ is the dissociation constant. Second, we take the limit of fast binding and fast diffusion ($K_A, \tilde{D} \rightarrow \infty$) with $\tilde{D}/K_A \rightarrow D_A$ and $\tilde{D}/K_B \rightarrow D_A K_r$, where we introduced $K_r = K_A/K_B$ as the ratio of the dissociation constants of the two isoforms. Adding now Eq. (3a) and Eq. (3b) and inserting Eq. (4), we obtain one advection-diffusion equation for each isoform, describing the effective dynamics of the bound myosin motors,

$$\partial_t c_A = -\partial_x(v c_A) + D_A \partial_x \mathcal{D}_A(c_A, c_B), \quad (5a)$$

$$\partial_t c_B = -\partial_x(v c_B) + D_A K_r \partial_x \mathcal{D}_B(c_A, c_B). \quad (5b)$$

Above, we have already dropped the indices a and in the following motors always refer to attached motors. The fact that the detached motor concentration drops out comes at the cost of concentration-dependent diffusion coefficients, which read

$$\begin{aligned} \mathcal{D}_i &= D_{ii} \partial_x c_i + D_{ij} \partial_x c_j \\ &= \frac{c_\infty (c_\infty - c_j)}{(c_\infty - (c_A + c_B))^2} \partial_x c_i + \frac{c_\infty c_i}{(c_\infty - (c_A + c_B))^2} \partial_x c_j. \end{aligned} \quad (6)$$

The diffusion for both (actin-bound) myosin isoforms is non-linear in the concentration, and it shows cross-diffusion properties, i.e. a gradient of isoform B influences the dynamics of isoform A and vice versa. Note that for $c_A = c_B = c/2$, we obtain the model for a single motor species interacting through volume exclusion [22]. The concentration dependence in the prefactors of the gradients in Eq. (6) arise from the excluded volume interaction, quantified by the saturation concentration c_∞ . For concentrations approaching saturation

the diffusion diverges, whereas for $c_A, c_B \ll c_\infty$ we recover concentration-independent diffusion constants and vanishing cross-coupling.

Both nonlinear diffusion and cross-diffusion have been introduced and analyzed for other systems, the former for instance for bacterial growth [29] and crowded motor protein systems [22, 30], the latter in micelle solutions [31], protein-polymer mixtures [32] and reaction-diffusion systems [33]. We here intend to investigate their effects in the context of intracellular flow, internal cell organization, cell polarization and cell motility.

C. Myosin as Tonks gas

The nonlinear, concentration-dependent diffusion of Eq. (6) can also be derived using arguments from classical irreversible thermodynamics. Assuming a homogeneous "gas" of two species A, B of hard spheres interacting only sterically (Tonks gas [23]), one finds a free energy density of

$$\begin{aligned} f(c_A, c_B) &= RT \left[c_A \ln \left(\frac{c_A}{c_\infty - c_A - c_B} \right) \right. \\ &\quad \left. + c_B \ln \left(\frac{c_B}{c_\infty - c_A - c_B} \right) + c_\infty \ln \left(1 - \frac{c_A + c_B}{c_\infty} \right) \right]. \end{aligned} \quad (7)$$

Here R is the universal gas constant and T temperature. This expression can be derived by either using a density functional theory ansatz [34–37] or statistical arguments similar to Flory-Huggins theory [38, 39].

The first two terms in Eq. (7) arise from a Tonks gas with two different species of spheres. However, the last term takes its form due to the introduction of holes into the system. These holes effectively constitute a third species. Besides, the cytosol and actin network are considered as an additional dense solvent background, whose influence can be neglected due to the myosin size. The saturation concentration then reads $c_\infty = c_A + c_B + c_{\text{holes}}$. In the dilute limit, i.e. for large c_∞ , the last term reduces to the sum of c_A and c_B which resembles the free energy of the combination of two individual Tonks gases. Hence, the last term can be interpreted as the correlation between both species at concentrations of an order of magnitude similar to the saturation.

Within nonequilibrium thermodynamics, fluxes are driven by gradients in conjugate thermodynamic forces. The relevant couple in our case is particle flux and chemical potential. In linear theory, the particle flux is expanded to linear order and can be associated with the diffusion within the multicomponent mixture. For the gas of two species we obtain (in one spatial dimension) the relation

$$\frac{1}{RT} \sum_{j \in \{A, B\}} L_{ij} \left(-\frac{\partial \mu_j}{\partial x} \right) = - \sum_{j \in \{A, B\}} D_{ij} \left(\frac{\partial c_j}{\partial x} \right), \quad (8)$$

where μ is the chemical potential, L_{ij} is the matrix of phenomenological coefficients and D_{ij} the diffusion matrix. Obtaining the chemical potential from the free energy via $\mu_j = \partial f / \partial c_j$, we get the same diffusion coefficients as derived from binding kinetics, Eq. (6), if the matrix of phenomenological coefficients is

$$\mathbf{L} = \frac{c_\infty}{c_\infty - c_A - c_B} \begin{pmatrix} c_A & 0 \\ 0 & c_B \end{pmatrix}. \quad (9)$$

The concentration-dependent prefactor of Eq. (9) arises due to the excluded volume interaction. It is necessary in order for the steric repulsion not to vanish in the limiting case of one of the species' concentration vanishing. Note that a species is not only affected by the excluded volume with itself, but also with the other species. For the dilute limit, which implies a large saturation concentration, the prefactor converges to unity and one recovers the diagonal matrix $L_{ij} = c_i \delta_{ij}$ as typically used for the diffusion of different species without explicit volume exclusion interactions, cf. e.g. Ref. [40].

D. Full Boundary Value Problem

By combining the myosin dynamics Eq. (5), with diffusion coefficients given by Eq. (6), with the constitutive relation, Eq. (1), and the force balance, Eq. (2), we can formulate the full boundary value problem.

We introduce dimensionless variables and rescale length and position by the cell length L_0 , time by L_0^2/D_A and contractile stress by the spring constant k . The concentrations are normalized using the initial average concentration of isoform A, i.e. $c_A^0 = \int c_A dx / L_0$. The initial average concentration of B can then be calculated using the relative abundance $c_r = c_A^0 / c_B^0$. Furthermore, we introduce $\mathcal{L} = \sqrt{\eta / (\xi L_0^2)}$ as the ratio of the viscous and the elastic length scales, the dimensionless contractility $P_i = \chi_i c_A^0 / k$ of the two isoforms and the Péclet number $Pe = k / (\xi D_A)$.

We then map the problem into internal coordinates $u = (x - l_-) / L \in [0, 1]$ to work on a fixed domain. The dimensionless boundary value problem then reads

$$-\frac{\mathcal{L}^2}{L^2} \partial_u^2 \tilde{\sigma} + \tilde{\sigma} = P_A \tilde{c}_A + P_B \tilde{c}_B, \quad (10a)$$

$$\partial_t \tilde{c}_A = -\frac{1}{L} \partial_u (\tilde{v} \tilde{c}_A) + \frac{1}{L^2} \partial_u \mathcal{D}_A (\tilde{c}_A / L, \tilde{c}_B / L), \quad (10b)$$

$$\partial_t \tilde{c}_B = -\frac{1}{L} \partial_u (\tilde{v} \tilde{c}_B) + \frac{K_r}{L^2} \partial_u \mathcal{D}_B (\tilde{c}_A / L, \tilde{c}_B / L). \quad (10c)$$

Here $\tilde{c}_i(u, t) = L(t) c_i(u, t)$ and $\tilde{\sigma}(u, t) = L(t) \sigma(u, t)$ are rescaled concentrations and stress. Both myosin isoform are advected by the actin retrograde flow with $\tilde{v} = \frac{Pe}{L^2} \partial_u \tilde{\sigma} - \dot{L} (u - \frac{1}{2}) - \dot{G}$. The elastic boundary condition reduces to $\tilde{\sigma}(u_\pm, t) = -L(t)(L(t) - 1)$ with $u_\pm \in \{0, 1\}$. The no-flux condition for the myosins is given by $\partial_u c_{A,B}(u_\pm, t) = 0$. The system of equations presented in Eq. (10) will now be analyzed in the following

by continuation methods and direct numerical simulation. The main parameters are Pe , P_A , P_B , K_r , c_∞ , c_r . The meaning of \mathcal{L} has been discussed before in [21, 22].

III. RESULTS

A. Comparison to One-Species Models

As a background for the new two-species model, we briefly recall the basic features of the one-species model. As studied in [19, 20], the model for one species and a constant diffusion coefficient allows for a supercritical pitchfork bifurcation from sessile to moving cells as a function of Pe . The instability is due to the motors being advected to and accumulating at the back, breaking the symmetry. The fact that the motor distribution is strongly peaked at the trailing end motivated the addition of excluded volume in Ref. [22], implying nonlinear diffusion (namely an increase of diffusion close to crowding) which smoothens the motor distribution. There, it was also shown that attractive interactions, modelling myosin mini-filament assembly, can render the bifurcation from supercritical to subcritical, thus leading to bistability and the possibility of optogenetic switching.

Here we are motivated by the experiments by Weissenbruch et al. [12, 16], who have investigated the distributions of the isoforms NMIIA and NMIIIB in polarized U2OS cells moving on a substrate in a steady fashion. As shown in Fig. 1, the more abundant, faster isoform A accumulates at the leading edge while the stronger, higher duty ratio NMIIIB at the trailing edge. Therefore we now have generalized this model to two species. For the moment being, we did not include any attraction yet, thus our reference case is the Tonks gas and not the van der Waals fluid.

B. Model Parameters

Informed by experimental data on crawling cells, we first estimate the parameters of our model. Due to $\xi \sim 2 \times 10^{14} Pa \text{ s m}^{-1}$ [22, 41], $\eta \sim 10^5 Pa \text{ s}$ [20, 41], $k \sim 10^4 Pa$ [16, 42, 43] and $L_0 \sim 20 \mu m$ [20] we obtain a (squared) relative viscous timescale of $\mathcal{L}^2 = 1.25$. Using $D_A \sim 0.1 \times 10^{-12} m^2 \text{ s}^{-1}$ [44–47], we infer the order of magnitude of the Péclet number to be $Pe \sim 100$.

The isoform-specific (off-)binding rates determine K_r , which in turn serves as a measure of relative diffusion. While the binding rates of both isoforms are equal ($k_{A,on} = k_{B,on} = 0.2 s^{-1}$), off-binding rates are $k_{A,off} = 1.71 s^{-1}$ and $k_{B,off} = 0.35 s^{-1}$ [27, 28, 48, 49] leading to a relative diffusion of $K_r \approx 0.2$. The contractility parameters, as defined earlier, are of the order $P_i \sim 0.1$ [20]. Due to the different duty ratios of the isoforms A and B we find $P_B \approx 3.6 \cdot P_A$ [27] and, thus, choose $P_A = 0.05$ and $P_B = 0.18$. Lastly, following arguments from Ref. [22] we use $c_\infty = 4$ for the saturation

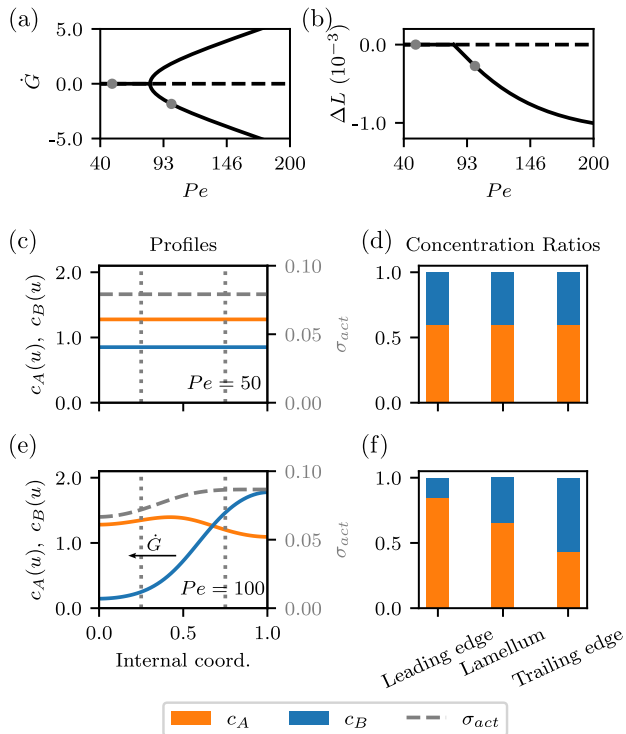


FIG. 2. Simulation results for steadily moving cells. (a) Supercritical pitchfork bifurcation of cell velocity \dot{G} as a function of the Péclet number Pe (primary continuation parameter). Solid lines mark stable, dashed lines unstable solutions. (b) Deviation of the cell length from its homeostatic value $\Delta L = L - L_0$ as a function of Péclet number. (c) Myosin concentration profiles of the two isoforms and the resulting total active stress σ_{act} of a sessile steady state. (d) The corresponding concentration ratios subdivided into three compartments as indicated by the gray dotted lines in (c). (e) Concentration profiles and total active stress for a motile steady state (cell velocity direction to the left indicated with arrow) and the corresponding concentrations ratios in (f). Parameters used: $\mathcal{L}^2 = 1.25$, $K_r = 0.2$, $P_A = 0.05$, $P_B = 0.18$, $c_\infty = 4$, $c_r = 1.5$.

concentration. The concentration ratio of $c_r \approx 1.5$ is taken from experiments [12].

C. Myosin Isoform Distributions in Steadily Moving Cells

We solve the boundary value problem for steady states using the numerical continuation software *Auto07-p* [50]. The results for the parameters estimated above are shown in Fig. 2. Panel (a) and (b) show the bifurcation diagrams. Below a critical value of $Pe_{crit} \approx 82$, the cell is in a sessile state with zero velocity (a) and at its homeostatic length (b). The corresponding concentration profiles are shown in panel (c): they are flat and hence symmetric for both isoforms. In (c) we also show the total active stress $\sigma_{act}(u) = -\chi_A c_A(u) - \chi_B c_B(u)$ as the

dashed line, which obviously is also flat. We also define the concentration ratios as $c_i/(c_A + c_B)$, with $i = A, B$.

At the critical Péclet number, a supercritical pitchfork bifurcation occurs, where the sessile state becomes unstable and stable motile steady states emerge. The two motile branches in panel (a) are \pm -symmetric and belong to the same, slightly contracted branch of the cell's length in panel (b). Whether one moves to the right or to the left is determined by the initial conditions. In the steadily moving cell state beyond the bifurcation, the myosin distributions are asymmetric, as depicted in panel (e). This symmetry break in the concentrations induces a polarized active stress profile that initiates cell polarization and motility. In the shown example, the active stress is highest at the right edge ($u = 1$), causing a negative velocity of the cell. The trailing edge is the locus of highest myosin concentration and, thus, highest active stress, in agreement to earlier theoretical works [20, 21] as well as experimental findings [12, 14, 16].

As already discussed, the two myosin isoforms and hence the concentration ratios are homogeneously distributed within the sessile state, see Fig. 2 (d). Comparing to Fig. 1 (d), due to the lack of a polarization axis in the sessile state, we should identify the lamellum with the cell center and the region called "intermediate" region in Fig. 1 (d), and both edges with the periphery. In the motile steady state the stronger isoform B sits in the back, while the more diffusive isoform A is displaced towards the front causing the varying concentration ratios as shown in panel (f). This redistribution is due to the retrograde flow, which is towards the trailing edge and during which motors unbind from actin. The higher the diffusion, the less motors of the respective isoform arrive at the trailing edge. For the estimated value of $K_r = 0.2$, isoform A has a larger effective diffusion than isoform B. Thus, B accumulates more quickly at the trailing edge. The effect of excluded volume then constrains A to accumulate further up front. The obtained results capture the experimental data from Weissenbruch et al. [12] qualitatively very well, compare Fig. 2(f) and Fig. 1(c).

D. Exploring Parameter Space and Occurrence of Oscillations

We now lift the constraint of steady states, solving the full boundary value problem Eq. (10) numerically, and explore the parameter space beyond the values estimated from experiments. The most interesting parameter to study is the ratio of the dissociation constants, K_r , which directly translates into the ratio of the diffusion constants of the two isoforms, cf. Eq. (5). The case discussed in the previous section corresponded to a low $K_r = 0.2$. We now consider a large $K_r = 10$ and fix the concentration ratio to $c_r = 1$ to focus on the effect of the reaction constants.

In this parameter regime, we find additional modes of motility, in particular the possibility of oscillations, as shown in Fig. 3. As before, for small Péclet number

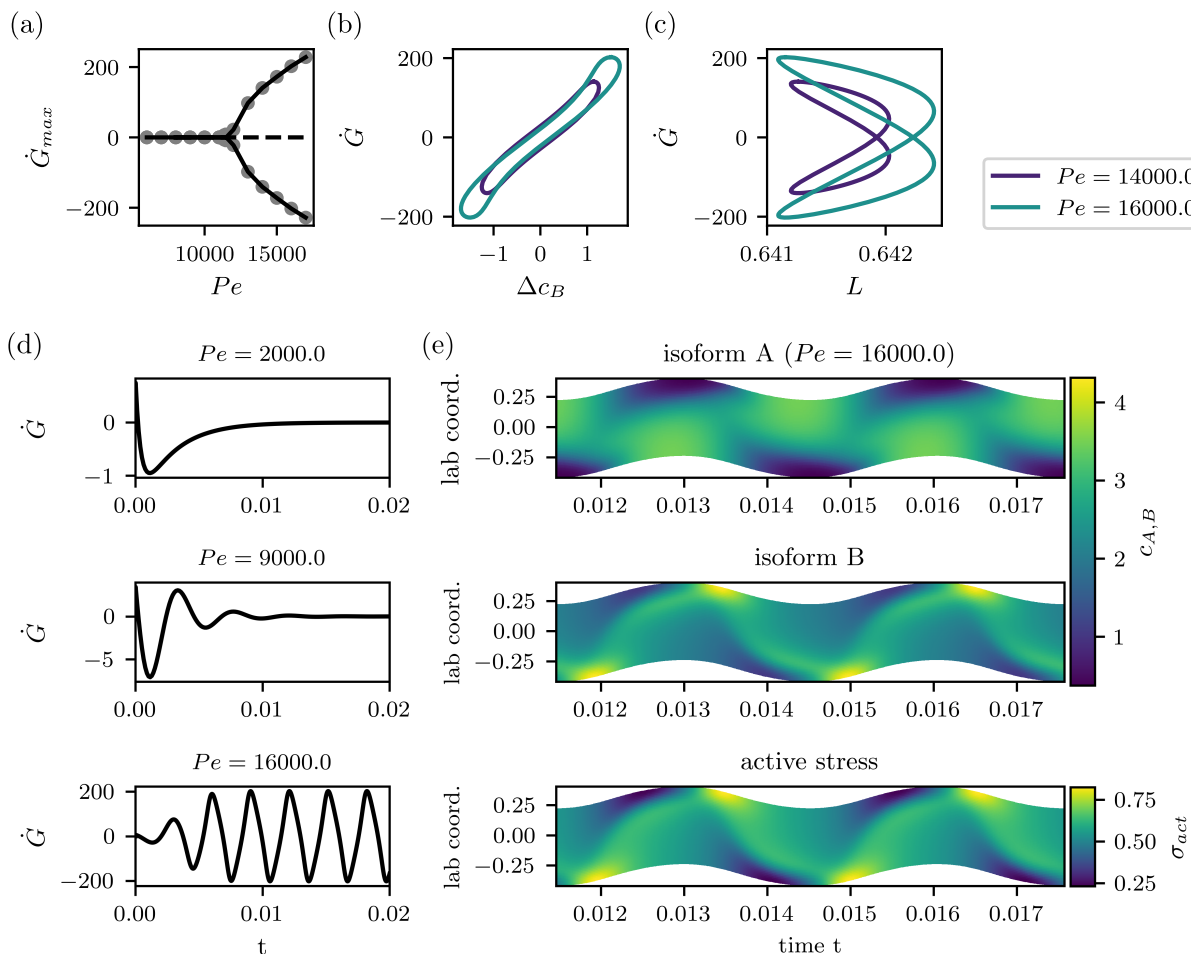


FIG. 3. Oscillatory dynamics of the two isoform system. (a) Hopf bifurcation at $K_{crit} = 11500$ in the \dot{G}_{max} - Pe -plane, where \dot{G}_{max} refers to the maximum velocity within an oscillation cycle. (b) Exemplary limit cycles in the \dot{G}_{max} - Δc_B -plane, where $\Delta c_B = c_B(l_+) - c_B(l_-)$ is a measure of the polarity of the myosin B distribution. The size of the limit cycle grows with Pe . (c) Exemplary limit cycles in the plane cell velocity vs. cell length. (d) Examples of the three different motility modes – sessile, transient oscillation and stable oscillation. Shown is the cell velocity over time. (e) Kymographs visualizing the pull-push-mechanism. Shown are the distributions of both myosin isoforms (upper and middle panel) and the resulting total active stress (lower panel) in a stable oscillatory state at $Pe = 16000$. Parameters as in Fig. 2, except for concentration ratio of $c_r = 1$ and strongly increased dissociation/diffusion ratio $K_r = 10$.

Pe we find stable sessile steady states. Increasing Pe leads to the onset of transient oscillations, whose amplitudes decay back to the sessile steady state in the regime $6000 \lesssim Pe \lesssim 11500$. Beyond a critical value of $Pe_{crit} \approx 11500$, these oscillations prevail and become stable. This behavior can be traced back to a Hopf bifurcation as shown in Fig. 3(a)-(c). Examples for the three different modes of motility – sessile, transient oscillation and stable oscillation – are shown in Fig. 3 (d).

For the oscillations to occur, the system requires a larger Péclet number. The increase of the critical Péclet number for the bifurcation as compared to Fig. 2 can be traced back to the increase of the effective diffusion of B (by a factor of 50) and the scaling of the Péclet number with the squared inverse of diffusion. The combination

of the bifurcation diagram, cf. panel (a), and the growing closed limit cycles, cf. panel (b) and (c), demonstrate the emergence of a supercritical Hopf bifurcation towards stable oscillations. Compared to the cell velocity oscillations, the oscillations in cell length are smaller by several orders of magnitude, see panel (c).

It is also interesting to study the polarity, which can be quantified by the left-right edge difference of the stronger motor $\Delta c_B = c_B(1) - c_B(0)$. The polarity and the velocity oscillate with the same frequency, see Fig. 3 (b), while the length oscillates with twice the frequency of the velocity oscillation, Fig. 3 (c). This is because in each cycle the cell passes every length twice, once during contraction and once during elongation.

How can the mechanism of the oscillation be under-

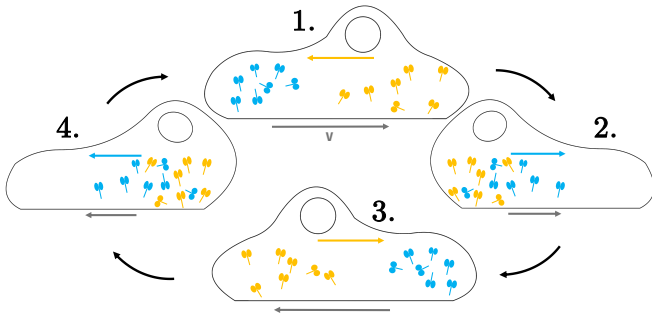


FIG. 4. Schematic sketch of myosin dynamics within an oscillating cell. (1) The cell initially moves to the right. More contractile species B (blue) at the back causes net flow of A (yellow) to the left. (2) Then A displaces B. Net flow of B to the right (blue arrow). (3) Cell movement slows down and reverses. Cycle of "pull-and-push" starts in the other direction.

stood? One has to note that for K_r large, one myosin isoform – namely myosin B – is both more contractile and more diffusive. If we assume initially a spatial separation of both isoforms, the stronger isoform B then induces a larger – and hence dominating – contractile stress that induces an actin flow towards the position where isoform B is the most aggregated. Myosin motors of isoform A are advected along the retrograde actin flow. As an effect of volume exclusion, isoform A subsequently displaces the more diffusive isoform B from its initial position and effectively "pushes" it to the other side of the cell. From this point on the pull-and-push cycle repeats. A schematic sketch of the internal myosin dynamics during one oscillation cycle is depicted in Fig. 4.

This pull-push mechanism is clearly visible within the simulation data in Fig. 3(e), showing kymographs (space-time-plots) of both isoforms (upper and middle panel) and the total active stress (lower panel) driving the dynamics. One can see that both isoforms continuously exchange positions which in turn corresponds to an oscillatory active stress. Within the lab frame, the cell oscillates in space and velocity. As the oscillation in cell length are much smaller than the one in cell velocity, it is barely visible in the kymographs.

Increasing $Pe \gtrsim 17000$, our numerics, using a Finite Volume Method implemented with the *FiPy*-package for *python* [51], became numerically unstable. The reason is that at such high Péclet number, advection dominates the diffusion and causes a lack of regularization. A code better adapted to the hyperbolic nature of this regime could be developed. We have rather chosen to circumvent this numerical problem by considering the rigid limit of the boundary value problem in the following, which also sheds new light on the origin of the oscillation and allows to establish a state diagram for the system.

E. The Rigid Limit and the State Diagram

The much smaller oscillation amplitude of the cell length compared to the cell velocity, cf. Fig. 3(c), suggests to look at the rigid limit of the problem, i.e. where the cell has constant length, to simplify the analysis.

Similarly as suggested in Ref. [20], we introduce a new dimensionless stress $\sigma' = \sigma/(c_A^0 \chi_A)$ leading to a new parameter for relative contractility $\chi_r = \chi_A/\chi_B$ and a new continuation parameter $\lambda = Pe P_A$. All other parameters from Eqs. (10) remain unchanged. The stiff limit then requires the contractility to be so small that the cell is not contracted, i.e. $P_{A,B} \rightarrow 0$, $L \rightarrow 1$. This leads to the adjusted elastic boundary condition

$$\sigma'(l_{\pm}, t) = \lim_{P_A \rightarrow 0} \lim_{L \rightarrow 1} \left(-\frac{1}{P_A} (L - 1) \right) =: \sigma_0, \quad (11)$$

where we assume the parameter σ_0 to be finite and implicitly defined through the remaining boundary conditions. We thus exchange the dynamics of the length, L , with the one from an implicitly defined "background stress" σ_0 , which encodes the changes in the averaged level of contraction.

To simplify the problem we introduce the stress deviation field $s(u) = \lambda(\sigma'(u) - \sigma_0)$. In internal coordinates, the new boundary value problem now reads

$$-\mathcal{L}^2 \partial_u^2 s + s + s_0 = \lambda \left(c_A + \frac{1}{\chi_r} c_B \right), \quad (12a)$$

$$\partial_t c_A = \partial_u \left[\left(\dot{G} - \partial_u s \right) c_A \right] + \partial_u \mathcal{D}_A(c_A, c_B), \quad (12b)$$

$$\partial_t c_B = \partial_u \left[\left(\dot{G} - \partial_u s \right) c_B \right] + K_r \partial_u \mathcal{D}_B(c_A, c_B), \quad (12c)$$

where $s_0 = \lambda \sigma_0$ and the diffusion coefficients are the ones from Eq. (6). The boundary conditions now read $\partial_u c_{A,B}(u_{\pm}, t) = s(u_{\pm}) = 0$ and $\partial_u s(u_{\pm}) = \dot{l}_{\pm} \equiv \dot{G}$. Note that albeit having set the length to a constant value, which makes Eqs. (12) much simpler than Eqs. (10), we have not lost its degree of freedom, which is now encoded in the background stress s_0 .

We can now perform a linear stability analysis, i.e. we expand all variables of our system in terms of small time- (and space-) dependent perturbations, added to the homogeneous steady state

$$s_0(t) = s_0^0 + \delta s_0(t), \quad (13a)$$

$$s(u, t) = s^0 + \delta s(u, t), \quad (13b)$$

$$c_i(u, t) = c_i^0 + \delta c_i(u, t), \quad i = A, B. \quad (13c)$$

We now neglect any dynamics of the background stress by assuming $\delta s_0(t) \equiv 0$. From the stress boundary condition, we can infer $s^0 = 0$. The equilibrium values for the isoforms are chosen, as before, to be $c_A^0 = 1$ and $c_B^0 = c_A^0/c_r$. When solving Eqs. (12) numerically using the FVM, we however keep the dependence on the background stress. It then has to be determined

for every time step, such that all boundary conditions are satisfied. In the analytical treatment, the perturbations are decomposed into Fourier modes of the form $[X_i(q_i) \cos(q_i u) + Y_i(q_i) \sin(q_i u)] e^{\sigma_q t}$ that have to satisfy the boundary conditions, leading to

$$\delta s = Y_s(2n\pi) \sin(2n\pi u) e^{\sigma_q t}, \quad (14a)$$

$$\delta c_A = X_A(n\pi) \cos(n\pi u) e^{\sigma_q t}, \quad (14b)$$

$$\delta c_B = X_B(n\pi) \cos(n\pi u) e^{\sigma_q t}. \quad (14c)$$

The spectrum of wave vectors is discrete with $n \in \mathbb{N}$ as we consider the finite domain $u \in [0, 1]$. Expanding the system of Eqs. (12) to linear order in the perturbations and inserting Eqs. (14) we obtain an eigenvalue problem $\sigma_q \mathbf{X} = \mathbf{M}_q \mathbf{X}$ for the vector $\mathbf{X} = (\delta s, \delta c_A, \delta c_B)$, with the matrix

$$\mathbf{M}_q = \begin{pmatrix} -4\mathcal{L}^2 q^2 - 1 & \lambda & \lambda/\chi_r \\ 4c_A^0 q^2 & -q^2 \frac{(c_\infty - c_B^0)}{\zeta_h} & -q^2 \frac{c_A^0}{\zeta_h} \\ 4c_B^0 q^2 & -q^2 K_r \frac{c_B^0}{\zeta_h} & -q^2 K_r \frac{(c_\infty - c_A^0)}{\zeta_h} \end{pmatrix}. \quad (15)$$

In the submatrix of the myosin concentrations, we introduced the common factor $\zeta_h = (c_\infty - c_A^0 - c_B^0)^2 / c_\infty$ coming from the nonlinear diffusion. The construction of the matrix \mathbf{M}_q through first and second order partial derivatives with respect to the perturbed variables renders the constant term s_0^0 irrelevant.

To predict the different modes of motility, we have to solve the eigenvalue problem. It is important to note that Eq. (12a) does not have any time derivatives, hence we take $\sigma_q = 0$ in the first row of the characteristic equation. This effectively sets one eigenvalue to zero and we are left with a pair of eigenvalues that potentially are complex.

The results are shown in Fig. 5. As shown in panel (a), the numerical results of the full system of equations (12) – shown as background colors – agree very well with the linear stability analysis (curves). This a posteriori justifies the neglect of perturbations in s_0 . We can identify four different modes of motility: sessile steady states, oscillations decaying towards a sessile steady state (transient oscillations), stable oscillations and motile steady states. Exemplary plots of velocity as a function of time for each of these modes are shown in panel (c).

As also obvious from Fig. 5(a), oscillations can only occur in case of $K_r > 1$. This implies $K_A > K_B$, meaning that the stronger isoform (myosin B) must have larger effective diffusion than the weaker isoform (myosin A). In the case of stable oscillations, we recover the pull-push mechanism that includes the consecutive displacement among both isoforms as shown in the kymograph of Fig. 5(b). This again proves the qualitative consistency of the rigid limit with the initial model, Eq. (10).

Note that in the linear analysis we have only used the first mode ($n = 1$), as it is the most dominant one for the dynamics: in fact, it is the first antisymmetric mode that creates the strongest polarity for δc_A and δc_B . Modes of even n do not produce cell motility as they create symmetric concentration profiles. Higher modes of odd

n cause antisymmetric concentration profiles that consist of multiple maxima/minima, leading to overall less polarity. Hence, the first mode suffices for a qualitative analysis of the dynamics of the systems, as also confirmed by the numerical solution. Also note that performing an analogous linear stability analysis for the original system Eq. (10) by simply fixing the length does not yield results consistent with the corresponding FVM simulations.

IV. DISCUSSION

Motivated by the existence of several isoforms of non-muscle myosin II (NMII), and specifically by the experiments by Weissenbruch et al. [12, 16], we have developed and analyzed a physical model including two interacting isoforms of NMII proteins. The interaction between the myosin isoforms A and B is mediated by excluded volume, that depends on the saturation concentration and leads to non-linear diffusion, derived both via a microscopic binding kinetics and non-equilibrium thermodynamics. The corresponding physics is that of a Tonks gas. In the future, one could also include an attractive interaction, thus changing to the van der Waals fluid as a reference case, as suggested earlier for a one-species active gel model [22]. We expect that such a model extension would change the bifurcation from supercritical to subcritical, leading to bistability and the possibility of optogenetic switching. Because this is not the focus of the current work and would make analytical progress even more difficult, here we here did not study this potential extension.

The two-species model introduced here recovers the experimental distributions of the isoforms and in addition predicts the existence of a variety of migratory modes. Regarding the steady states, in the non-motile steady state both isoforms are homogeneously distributed and cause a symmetric active contractile stress. At sufficiently large Péclet numbers, however, this symmetry is broken and polarized concentration fields and, consequently, polarized active stress profiles emerge. This onset of polarization and migration is due to a supercritical pitchfork bifurcation. For a steadily moving cell beyond the bifurcation, we find the experimentally observed, isoform-specific myosin distribution profiles [12]: the faster NMIIA accumulates at the leading edge, while the stronger NMIIIB localizes at the trailing edge.

We have explored further modes of motility besides the steady state solutions. Oscillations occur in case that the more contractile isoform is also more diffusive (i.e. $P_B > P_A$, $K_r > 1$), via a cyclic pull-push-mechanism. This mechanism works best for similar total abundances of both isoform, $c_r \sim 1$, which might be the reason why it has not been observed yet. It has been suggested that different myosin isoforms can be regulated independently [52–54], which would allow for the relative diffusion to be controlled via K_r . Albeit not observed in the cell type investigated in Refs. [12, 16], it is not unlikely that these

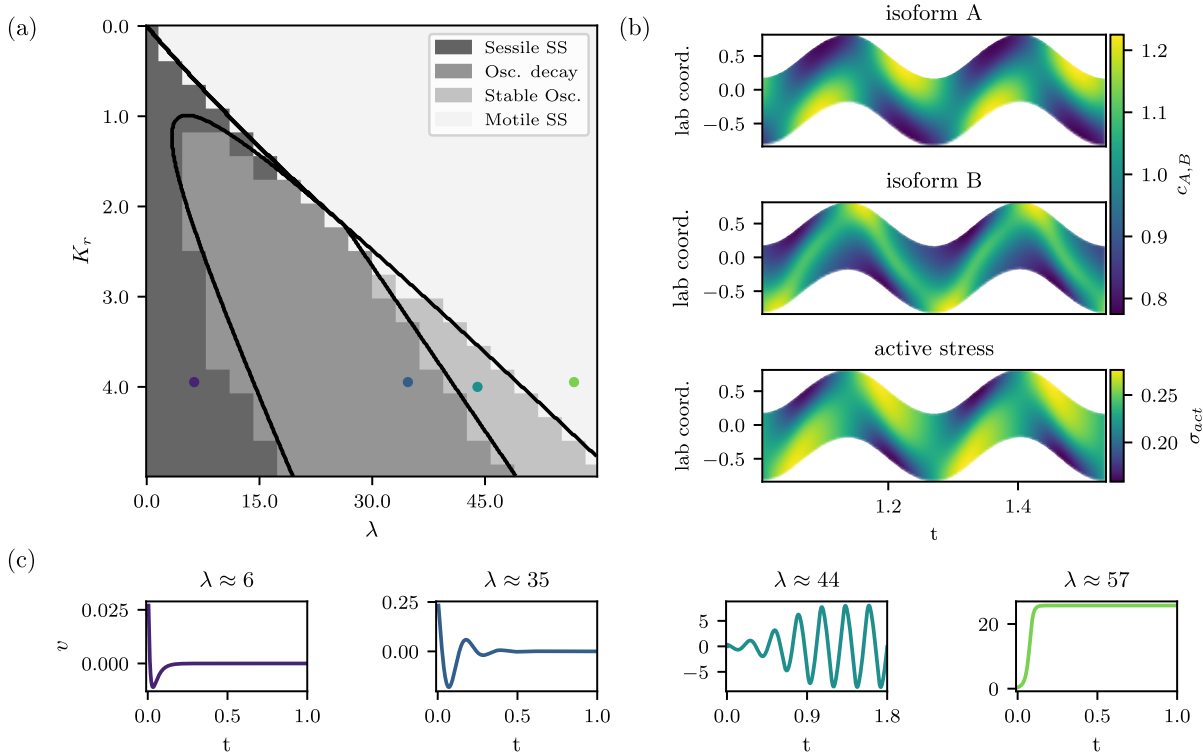


FIG. 5. Motility modes in the rigid limit. (a) State diagram of the four different motility modes depending on the relative diffusion K_r vs. the rescaled Péclet number λ . Numerical results obtained by FVM simulations of equations (12) are coded in levels of gray. The curves are obtained from the linear stability eigenvalue problem and mark analytically predicted borders of the state diagram. (b) Kymographs for the two motor isoform concentrations and the resulting total active stress in a state of stable oscillations ($\lambda = 44$). (c) Examples of the four different motility modes as plots of velocity over time. λ is varied while $K_r \approx 4$ was kept fixed. Parameters correspond to the points indicated in (a). Parameters not mentioned have the same values as in Fig. 3.

oscillations might occur in other cell types. They also could be induced by perturbations, either of the relative abundances or of the regulatory networks controlling actomyosin dynamics. In addition, the parameter c_r could be tuned using optogenetical activation of knock-downs.

In the oscillatory state, the amplitude of the cell length oscillation is much smaller than the one of velocity. This suggested to study the rigid limit, which enabled an analytic linear stability analysis and allowed to determine the full state diagram of the system, containing sessile cells, cells with transient oscillations and persistent oscillations, as well as steady motile cell solutions. This phase diagram is in good agreement with FVM simulations of the full model.

In summary, here we have shown that active gel theory can be extended to also describe the effect of having two complementary isoforms at work. The fact that we could derive the same model from both kinetic and a thermodynamic perspectives demonstrate its fundamental nature and paves the way to also include other biologically relevant effects into the model. In particular, a third major molecular constituent of contractile structures in cells is

α -actinin, which like NMII also exists in different isoforms and which also competes for binding to the actin filaments. In the future, it would be interesting to further extend active gel theory to such situations with multiple components.

V. ACKNOWLEDGMENTS

We thank Martin Bastmeyer and his group for helpful discussions. O.M.D. acknowledges support by the Max Planck School Matter to Life supported by the German Federal Ministry of Education and Research (BMBF) in collaboration with the Max Planck Society. We also acknowledge support by the Deutsche Forschungsgemeinschaft (DFG, German Research Foundation, project numbers EXC 2181/1 - 390978043, EXC 2082/1-390761711 and SFB-1638/1 - 511488495 - P03). U.S.S. is member of the Interdisciplinary Center for Scientific Computing (IWR) at Heidelberg.

- [1] G. Reig, E. Pulgar, and M. L. Concha, Cell migration: from tissue culture to embryos, *Development* (Cambridge, England) **141**, 1999–2013 (2014).
- [2] X. Trepap, M. R. Wasserman, T. E. Angelini, E. Millet, D. A. Weitz, J. P. Butler, and J. J. Fredberg, Physical forces during collective cell migration, *Nat. Phys.* **5**, 426 (2009).
- [3] S. Nourshargh, P. L. Hordijk, and M. Sixt, Breaching multiple barriers: leukocyte motility through venular walls and the interstitium, *Nat. Rev. Mol. Cell Biol.* **11**, 366 (2010).
- [4] C. Stuelten, C. Parent, and D. Montell, Cell motility in cancer invasion and metastasis: insights from simple model organisms, *Nat. Rev. Cancer* **18**, 296 (2018).
- [5] L. Blanchoin, R. Boujemaa-Paterski, C. Sykes, and J. Plastino, Actin dynamics, architecture, and mechanics in cell motility, *Physiol. Rev.* **94**, 235 (2014).
- [6] A. B. Verkhovskiy, T. M. Svitkina, and G. G. Borisy, Self-polarization and directional motility of cytoplasm, *Curr. Biol.* **9**, 11 (1999).
- [7] A. J. Ridley, M. A. Schwartz, K. Burridge, R. A. Firtel, M. H. Ginsberg, G. Borisy, J. T. Parsons, and A. R. Horwitz, Cell migration: Integrating signals from front to back, *Science* **302**, 1704 (2003).
- [8] F. Ziebert, S. Swaminathan, and I. S. Aranson, Model for self-polarization and motility of keratocyte fragments, *J. R. Soc. Interface* **9**, 1084–1092 (2012).
- [9] A. Hadjithodorou, G. R. R. Bell, F. Ellett, S. Shastri, D. Irimia, S. R. Collins, and J. A. Theriot, Directional reorientation of migrating neutrophils is limited by suppression of receptor input signaling at the cell rear through myosin ii activity, *Nat. Commun.* **12**, 6619 (2021).
- [10] L. Valon, A. Marín-Llaurado, T. Wyatt, G. Charras, and X. Trepap, Optogenetic control of cellular forces and mechanotransduction, *Nat. Commun.* **8**, 14396 (2017).
- [11] K. Hennig, I. Wang, P. Moreau, L. Valon, S. DeBeco, M. Coppey, Y. A. Miroshnikova, C. Albiges-Rizo, C. Favard, R. Voituriez, and M. Balland, Stick-slip dynamics of cell adhesion triggers spontaneous symmetry breaking and directional migration of mesenchymal cells on one-dimensional lines, *Science Advances* **6**, eaau5670 (2020).
- [12] K. Weissenbruch, M. Fladung, J. Grewe, L. Baulesch, U. S. Schwarz, and M. Bastmeyer, Nonmuscle myosin iia dynamically guides regulatory light chain phosphorylation and assembly of nonmuscle myosin iib, *Eur. J. Cell Biol.* **101**, 10.1016/j.ejcb.2022.151213 (2022).
- [13] M. Vicente-Manzanares, X. Ma, Adelstein, and et al., Non-muscle myosin ii takes centre stage in cell adhesion and migration, *Nat. Rev. Mol. Cell Biol.* **10**, 778 (2009).
- [14] K. Weissenbruch and R. Mayor, Actomyosin forces in cell migration: Moving beyond cell body retraction, *Bioessays* 10.1002/bies.202400055 (2024).
- [15] J. R. Beach, L. Shao, K. Remmert, D. Li, E. Betzig, and J. A. Hammer, Nonmuscle myosin ii isoforms coassemble in living cells, *Curr. Biol.* **24**, 1160 (2014).
- [16] K. Weissenbruch, J. Grewe, M. Hippler, M. Fladung, M. Tremmel, K. Stricker, U. S. Schwarz, and M. Bastmeyer, Distinct roles of nonmuscle myosin ii isoforms for establishing tension and elasticity during cell morphodynamics, *eLife* (2021).
- [17] K. Kruse, J. F. Joanny, F. Jülicher, J. Prost, and K. Sekimoto, Asters, vortices, and rotating spirals in active gels of polar filaments, *Phys. Rev. Lett.* **92**, 078101 (2004).
- [18] K. Kruse, J. Joanny, F. Jülicher, and et al., Generic theory of active polar gels: a paradigm for cytoskeletal dynamics, *Eur. Phys. J. E* **16**, 5 (2005).
- [19] P. Recho, T. Putelat, and L. Truskinovsky, Contraction-driven cell motility, *Phys. Rev. Lett.* **111**, 108102 (2013).
- [20] P. Recho, T. Putelat, and L. Truskinovsky, Mechanics of motility initiation and motility arrest in crawling cells, *J. Mech. Phys. Solids* **84**, 469 (2015).
- [21] O. M. Drozdowski, F. Ziebert, and U. S. Schwarz, Optogenetic control of intracellular flows and cell migration: A comprehensive mathematical analysis with a minimal active gel model, *Phys. Rev. E* **104**, 10.1103/PhysRevE.104.024406 (2021).
- [22] O. M. Drozdowski, F. Ziebert, and U. S. Schwarz, Optogenetic control of migration of contractile cells predicted by an active gel model, *Communications Physics* **6**, 10.1038/s42005-023-01275-0 (2023).
- [23] L. Tonks, The complete equation of state of one, two and three-dimensional gases of hard elastic spheres, *Phys. Rev.* **50**, 955 (1936).
- [24] M. A. Geeves and K. C. Holmes, The molecular mechanism of muscle contraction, *Adv. Protein Chem.* , 161 (2005).
- [25] H. L. Sweeney and A. Houdusse, Structural and functional insights into the myosin motor mechanism, *Annu. Rev. Biophys.* , 539 (2010).
- [26] T. Erdmann, P. J. Albert, and U. S. Schwarz, Stochastic dynamics of small ensembles of non-processive molecular motors: The parallel cluster model, *J. Chem. Phys.* **139**, <https://doi.org/10.1063/1.4827497> (2013).
- [27] T. Erdmann, K. Bartelheimer, and U. S. Schwarz, Sensitivity of small myosin ii ensembles from different isoforms to mechanical load and atp concentration, *Phys. Rev. E* **94**, 10.1103/PhysRevE.94.052403 (2016).
- [28] S. Stam, J. Alberts, M. L. Gardel, and E. Munro, Isoforms confer characteristic force generation and mechanosensation by myosin ii filaments, *Biophys. J.* **108**, 1997 (2015).
- [29] J. Müller and W. Van Saarloos, Morphological instability and dynamics of fronts in bacterial growth models with nonlinear diffusion, *Phys. Rev. E* **65**, 061111 (2002).
- [30] H. Chelly and P. Recho, Cell motility as an energy minimization process, *Phys. Rev. E* **105**, 064401 (2022).
- [31] D. G. Leaist and S. M. Abdu, Ternary mutual diffusion coefficients and critical micelle concentrations of aqueous sodium dodecyl sulfate + lithium dodecyl sulfate solutions at 25°C, *J. Chem. Eng. Data* **46**, 922 (2001).
- [32] A. Vergara, L. Paduano, and R. Sartorio, Mechanism of protein-poly(ethylene glycol) interaction from a diffusive point of view, *Macromolecules* **35**, 1389 (2002).
- [33] V. K. Vanag and I. R. Epstein, Cross-diffusion and pattern formation in reaction-diffusion systems, *Phys. Chem. Chem. Phys.* **11**, 897 (2009).
- [34] P. Tarazona, J. Cuesta, and Y. Martinez-Raton, Density functional theories of hard particle systems, *Lect. Notes Phys.* **753**, 247 (2008).

- [35] P. Tarazona and Y. Rosenfeld, New approaches to problems in liquid state theory - inhomogeneities and phase separation in simple, complex and quantum fluids (NATO Science Series, 1998) Chap. free energy density functional from 0D cavities.
- [36] L. Lafuente and J. A. Cuesta, Elusiveness of fluid-fluid demixing in additive hard-core mixtures, *Phys. Rev. Lett.* **89**, 10.1103/PhysRevLett.89.145701 (2002).
- [37] L. Lafuente and J. A. Cuesta, Density functional theory for general hard-core lattice gases, *Phys. Rev. Lett.* **93**, 10.1103/PhysRevLett.93.130603 (2004).
- [38] P.-G. de Gennes, Scaling concepts in polymer physics (Cornell University Press, Ithaca London, 1979) Chap. 3: Polymer Solutions in Good Solvents.
- [39] K. A. Dill and S. Bromberg, Molecular driving forces - statistical thermodynamics in chemistry and biology (Garland Science, 2002) Chap. 31: Polymer Solutions.
- [40] T. Aslyamov, F. Avanzini, E. Fodor, and M. Esposito, Nonideal reaction-diffusion systems: Multiple routes to instability, *Phys. Rev. Lett.* **131**, 138301 (2023).
- [41] E. L. Barnhart, K.-C. Lee, K. Keren, A. Mogilner, and J. A. Theriot, An Adhesion-Dependent Switch between Mechanisms That Determine Motile Cell Shape, *PLoS Biol.* **9**, e1001059 (2011).
- [42] E. L. Barnhart, G. M. Allen, F. Jülicher, and J. A. Theriot, Bipedal Locomotion in Crawling Cells, *Biophys. J.* **98**, 933 (2010).
- [43] A. J. Loosley and J. X. Tang, Stick-slip motion and elastic coupling in crawling cells, *Phys. Rev. E* **86**, 031908 (2012), publisher: American Physical Society.
- [44] R. Uehara, G. Goshima, I. Mabuchi, R. D. Vale, J. A. Spudich, and E. R. Griffis, Determinants of Myosin II Cortical Localization during Cytokinesis, *Curr. Biol.* **20**, 1080 (2010).
- [45] T. Luo, K. Mohan, V. Srivastava, Y. Ren, P. A. Iglesias, and D. N. Robinson, Understanding the Cooperative Interaction between Myosin II and Actin Cross-Linkers Mediated by Actin Filaments during Mechanosensation, *Biophys. J.* **102**, 238 (2012).
- [46] J. Kolega and D. L. Taylor, Gradients in the concentration and assembly of myosin II in living fibroblasts during locomotion and fiber transport., *Mol. Biol. Cell* **4**, 819 (1993).
- [47] Y. Chen, D. Saintillan, and P. Rangamani, Interplay Between Mechanosensitive Adhesions and Membrane Tension Regulates Cell Motility, *PRX Life* **1**, 023007 (2023).
- [48] S. Walcott, D. M. Warshaw, and E. P. Debold, Mechanical coupling between myosin molecules causes differences between ensemble and single-molecule measurements, *Biophys. J.* **103**, 501 (2012).
- [49] A. Vilfan and T. Duke, Instabilities in the transient response of muscle, *Biophys. J.* **85**, 818 (2003).
- [50] E. J. Doedel and B. E. Oldeman, Auto-07p : Continuation and bifurcation software for ordinary differential equations (2012).
- [51] J. Guyer, D. Wheeler, and J. Warren, Fipy: Partial differential equations with python, *Comput. Sci. Eng.* **11**, 6 (2009).
- [52] A. R. Bresnick, Molecular mechanisms of nonmuscle myosin-ii regulation, *Curr. Opin. Cell Biol.* **11**, 26 (1999).
- [53] B. Barua, D. A. Winkelmann, H. D. White, and S. E. Hitchcock-DeGregori, Regulation of actin-myosin interaction by conserved periodic sites of tropomyosin, *PNAS* **109**, 18425 (2012).
- [54] J. E. Clayton, M. R. Sammons, B. C. Stark, A. R. Hodges, and M. Lord, Differential regulation of unconventional fission yeast myosins via the actin track, *Curr. Biol.* **20**, 1423 (2010).